

Analysis of Strengthening Mechanisms in Nano-ODS Steel Depending on Preparation Route

Alessandra Fava^{1*}, Roberto Montanari¹, Maria Richetta¹, Claudio Testani² and Alessandra Varone¹

¹Department of Industrial Engineering, University of Rome "Tor Vergata", Via del Politecnico, Rome, Italy

²CALEF-ENEA CR Casaccia, Via Anguillarese, Santa Maria di Galeria, Rome, Italy

Abstract

Oxide dispersion strengthened (ODS) steels are promising materials for high temperature applications, in particular in fission and fusion nuclear reactors. In comparison to common reduced activation ferritic/martensitic steels they exhibit better resistance to neutron irradiation and creep owing to an uniform dispersion of nano-oxides particles (~5 nm) and a very fine grain structure (~500 nm).

ODS steels are commonly prepared by high-energy mechanical alloying (HEMA) of a mixture of steel powder and Y_2O_3 particles followed by a consolidation stage consisting of hot extrusion (HE) or hot isostatic pressing (HIP). The samples are then submitted to annealing around 1100°C for 1-2 hours. Recently, the present authors proposed a novel method based on low-energy mechanical alloying (LEMA).

In general ODS microstructure is quite complex and several mechanisms contribute to the mechanical strengthening with different effects depending on the temperature. The present work analyses the role played by each single mechanism at increasing temperature by considering the specific microstructural features.

ODS steels prepared through different routes and process parameters display different grain size distribution and homogeneity of particles dispersion, factors which strongly affect the mechanical properties.

Yield stress values measured in tensile tests performed at increasing temperature up to 700°C, either taken from literature or achieved by authors, have been examined and the following strengthening mechanisms have been considered to fit the experimental data: (i) solid solution; (ii) Bailey-Hirsch; (iii) Hall-Petch; (iv) Orowan; (v) Coble creep and (vi) Arzt-Rösler-Wilkinson. The analyses evidence advantages and drawbacks of different preparation routes and suggest some criteria for further improving the mechanical properties of these materials.

Keywords: ODS steel; Nanostructure; Mechanical alloying; Mechanical properties; Strengthening mechanisms

Introduction

During the last decades, the design of fusion and generation IV nuclear reactors has led to the development of alternative materials for structural components in the reactors [1,2]. The reduced activation ferritic/martensitic (RAFM) steels are considered the most suitable option as structural materials owing to the well-known manufacturing process of the steel production and their good thermomechanical properties and resistance to neutron irradiation [3-6]. Nevertheless the RAFM steels present some drawbacks such as: i) the degradation of the mechanical properties above 550°C; ii) drop of creep resistance above 550°C and iii) effects of hardening and embrittlement owing to the great amount of helium and hydrogen produced under irradiation conditions (at $T < 400^\circ\text{C}$) [6-9]. Therefore, oxide dispersion strengthened (ODS) steels were developed to reinforce the steel matrix of the RAFM steels with a dispersion of oxides particles [4,10,11]. The strengthening of ODS steels is achieved by the combination of a uniform dispersion of fine oxides, mostly Y_2O_3 particles, and a sub-micrometrical grain structure (~500 nm). The former mechanism is due to the oxide particles that act as obstacle preventing the dislocation motion and hindering recovery and recrystallization, the latter one is well described by the Hall-Petch equation [12-14]. Furthermore, in order to refine the size of oxide particles small amounts of titanium are added in the steel matrix with consequent formation of fine Y-Ti-O particles (size from 2 to 10 nm) [11,15]. All these characteristics improve the mechanical properties up to ~800°C, the creep resistance, the corrosion resistance and increase the resistance to irradiation damage, i.e., swelling, embrittlement and damage accumulation [16-20].

The most conventional route to manufacture ODS steels is the high-energy mechanical alloying (HEMA). A mixture of steel powders and Y_2O_3 particles is milled for about 20-60 hours at 300-500 rpm, so Y_2O_3 is decomposed into Y and O atoms which are then uniformly dissolved in the steel matrix. Hereafter, the samples are consolidated by hot extrusion (HE) or hot isostatic pressing (HIP) and a further annealing heat treatment at ~1100°C for 1-2 hours is carried out in order to bond the Y and O atoms with Ti and to precipitate Y-Ti-O nano-particles [11,21,22]. The method has a clear shortcoming because it leads to a bimodal grain size distribution with anisotropic mechanical properties [23,24]. To overcome such drawback and obtain a homogeneous grain size distribution present authors recently proposed a novel method based on low-energy mechanical alloying (LEMA), consolidation by hot extrusion (~1100°C) without the final annealing treatment [25]. In this work the microstructural and mechanical properties of an ODS steel produced by LEMA are compared with those of the same unreinforced steel and of ODS steels produced with the conventional route (HEMA). The analyses examine the contributions to strengthening of different mechanisms at increasing temperature up to 700°C: (i) solid solution

***Corresponding author:** Alessandra Fava, Department of Industrial Engineering, University of Rome "Tor Vergata", Via del Politecnico 1, 00133 Rome, Italy, Tel: +39-06-7259-7180; E-mail: alessandra.fava@uniroma2.it

Received July 26, 2018; Accepted August 02, 2018; Published August 12, 2018

Citation: Fava A, Montanari R, Richetta M, Testani C, Varone A (2018) Analysis of Strengthening Mechanisms in Nano-ODS Steel Depending on Preparation Route. J Material Sci Eng 7: 474. doi: [10.4172/2169-0022.1000474](https://doi.org/10.4172/2169-0022.1000474)

Copyright: © 2018 Fava A, et al. This is an open-access article distributed under the terms of the Creative Commons Attribution License, which permits unrestricted use, distribution, and reproduction in any medium, provided the original author and source are credited.

(σ_{SS}); (ii) Bailey-Hirsch (σ_{BH}); (iii) Hall-Petch (σ_{HP}); (iv) Orowan (σ_{OR}); (v) Coble creep (σ_{CC}) and (vi) Arzt-Rösler-Wilkinson (σ_{ARW}).

Materials and Methods

The ODS steel has been produced from a pre-alloyed steel powder prepared by vacuum gas atomization with the nominal chemical composition (wt%) reported in Table 1.

The steel powder consists of nearly spherical particles with bimodal size distribution peaked at 4 and 20 μm (Figure 1a) while the particles of Y_2O_3 reinforcement have a smaller size, lower than 50 nm (Figure 1b). The amount of Y_2O_3 in ODS steel is 0.3 wt%.

The steel powder and the reinforcement particles were processed through a large scale horizontally rotating low-energy dry-ball miller with a diameter of 200 mm and a capability of $6 \times 10^{-3} \text{m}^3$ using stainless steel balls (AISI 316) with two different diameters (10 mm and 2.5 mm). The stainless steel jar containing powder and balls (ratio 1:10) were put in rotation for 300 hours at 60 rpm in vacuum ($P \sim 10^{-4}$ mbar). In order to prevent the oxygen contamination during the mechanical alloying process, a glove box in Ar-2% H atmosphere was used to handle the powders and to seal the jar.

The energy ΔE transferred per hit and per unit of mass depends on the maximum quantity of trapped material (Q_{MAX}), radius of the planetary mill, ball material density, Young's modulus, rotation speed, ball diameter and surface density of the powder covering the balls [26]. If one considers a rotation speed of 300 rpm the value $\Delta E/Q_{MAX}$ is estimated to be ~ 11 J/g hit whereas it is about 7 times higher (~ 75 J/g. hit) in HEMA [25].

As shown in Figure 2, after LEMA process the morphology of

Element	wt%
Cr	14
W	1
Ti	0.4
Mn, Si	0.3
Ni	0.15
Cu	≤ 0.03
V	≤ 0.02
Mo, Al, C	≤ 0.01
N	≤ 0.007
P	≤ 0.008
S	≤ 0.001
Co, Ta	≤ 0.005
Nb, Sn, Sb, As, Ag	≤ 0.002
Fe	to balance

Table 1: Nominal chemical composition of the steel powder used to manufacture the ODS by means of LEMA.

powders drastically changes. The original particles of steel and Y_2O_3 are no more present and the new particles exhibit an irregular shape with an almost homogenous size of $\sim 35 \mu\text{m}$ (Figure 2a). For comparison, the mechanical alloyed steel powder without reinforcement are displayed in Figure 2b. They exhibit a bimodal size distribution similar to that of the original powder.

Powders after LEMA have been hot extruded at 1100°C.

A set of samples were studied in the as-prepared condition while another part were submitted to heat treatments at 1050, 1100 and 1150°C for 30 minutes (samples T1, T2, T3).

The microstructure and the chemical composition of oxide particles have been investigated by means of Transmission Electron Microscopy (TEM) and Energy-Dispersive X-ray spectroscopy (EDX). The samples have been firstly prepared by mechanical grinding and then thinned by a double-jet electrolytic polishing in a solution of 10% perchloric acid+90% ethylene glycol monobutyl ether at -20°C (30 V, 8.5 mA).

X-ray diffraction (XRD) spectra were recorded using Mo-K α radiation ($\lambda=0.07093$ nm) in step-scanning mode with 2θ steps of 0.05° and counting time of 5 s per step. From high precision peak profiles, collected with 2θ steps of 0.005° , the contributions to line broadening due to micro-strains ϵ and coherently diffracting domains were determined [27] and the dislocation density ρ calculated through the Williamson-Smallman equation [28]:

$$\rho = \frac{\Xi \epsilon^2}{k_0 b^2} \quad (1)$$

where $\Xi=16$ is a constant, $b=0.25$ nm the modulus of Burgers vector and $k_0 \cong 1$ a term depending on dislocation interaction.

The samples have been characterized by Vickers microhardness tests (100 g/10 s) and tensile tests at increasing temperatures up to 700°C made with a strain rate $\dot{\epsilon}=10^{-3} \text{s}^{-1}$. The gauge length and the diameter of the tensile specimens were 16.5 mm and 4 mm, respectively.

Through Mechanical Spectroscopy (MS) the shear modulus G has been measured in the temperature range 25-700°C. MS test runs were carried out by using the VRA 1604 apparatus [29] and bar-shaped samples (60 mm \times 7 mm \times 0.5 mm) mounted in free-clamped mode. The heating rate was 1°C/minute.

Results

Steel powder

In order to evaluate the specific hardening-effect induced by Y_2O_3 particle addition, some comparative experiments have been carried out on the powder with and without particle reinforcement. Both sets

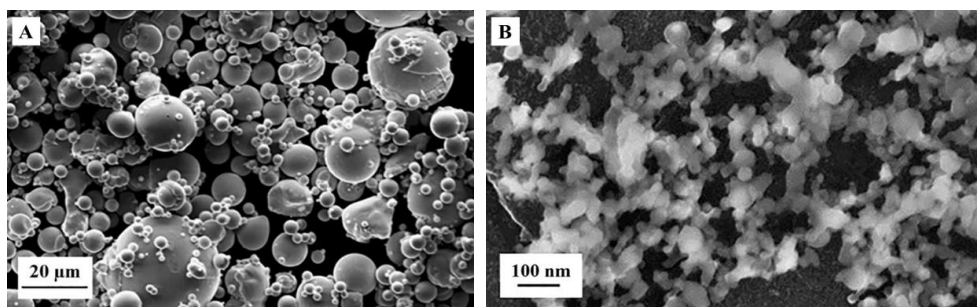


Figure 1: Powder of steel (a) and of Y_2O_3 (b).

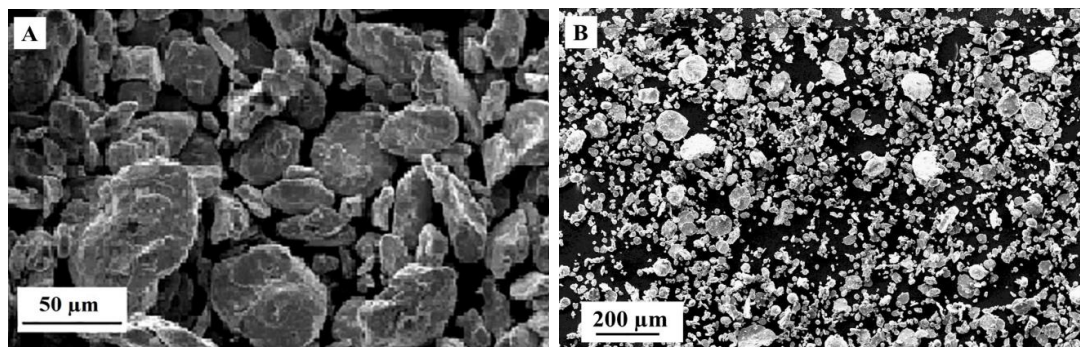


Figure 2: Morphology of powder after LEMA: mixture of steel and Y_2O_3 (a), only steel powder (b).

Sample	LEMA	Heat Treatment	Hardness (HV)
Steel powder	No	No	187 ± 6
Steel powder	Yes	No	363 ± 8
Steel powder	Yes	800°C/2 hours	172 ± 5
Steel powder+ Y_2O_3 particles	Yes	No	476 ± 10
Steel powder+ Y_2O_3 particles	Yes	800°C/2 hours	474 ± 10

Table 2: Hardness of LEMA steel powder with and without the reinforcement of Y_2O_3 particles before and after annealing at 800°C for 2 hours.

of steel powder have been submitted to LEMA, than heat treated at 800°C for 2 hours. Table 2 reports the results of microhardness tests on different samples.

The original hardness of steel powder is 187 HV and increases to 363 HV after LEMA. The hardening is completely recovered after the heat treatment thus it can be ascribed to lattice defects introduced by plastic deformation.

The hardness of the steel powder with Y_2O_3 is 476 HV, much higher than that of the steel powder without reinforcement subjected to LEMA in the same conditions. The extra hardening is the effect of mechanically activated diffusion phenomena leading to in-situ nano-precipitation of reinforcing complex oxides. More important, hardness is not affected by the heat treatment at 800°C. This suggesting that microstructural characteristics of the alloy i.e., volume fraction and dimension of hardening particles as well as the alloy grain size are not substantially altered at relatively high temperatures. The dislocation density is substantially the same before and after the heat treatment.

Hot extruded samples

XRD patterns recorded from samples consolidated through HE exhibit a narrowing of peak profiles with respect those from powders after LEMA. The peak profile analysis shows that the effect is due to the decrease of dislocation density occurring during the HE at 1100°C rather than a difference of grain size. The average size of coherently diffracting domains (i.e., the grains) resulted to be about 400 nm for both ODS steel and mechanical alloyed powder whereas the dislocation densities are $4 \times 10^{12} m^{-2}$ and $7.4 \times 10^{12} m^{-2}$, respectively. Therefore, HE induces a partial recovery of dislocation structures but is not able to significantly change the mean grain size.

XRD results are confirmed by TEM observations (Figure 3). The microstructure of the ODS steel after HE consists of equiaxed ferritic grains with an average size of ~400 nm thus the novel method based on LEMA and successive HE consolidation without the final annealing treatment is able to avoid the bimodal grain size distribution, typical microstructural feature resulting from the conventional method of ODS production.

The dislocation density is not homogeneous: in some grains it is lower (Figure 3b), in others higher (Figure 3c). Therefore, it is reasonable that also microstrains are not homogenous in the material.

TEM analysis reveals also the presence of different types of precipitates (Figure 4). The particles indicated with points from 1 to 5 in Figure 4a and 4b are oxides with a round or irregular shape and size commonly ranging from 30 to 100 nm, even if some of them reach ~300 nm. The EDX analysis evidences that they are complex oxides containing different amounts of alloying elements. For example, Table 3 reports the compositions measured on the particles 1-5 in Figure 4a.

Moreover, it is observed a massive precipitation of very small (few nanometers) particles with squared shape within the ferritic grains and along the grain boundaries (Figure 4c and 4d). The presence of this type of precipitates confirms that the addition of small percentages of titanium in the steel composition contributes to the precipitation of nanometric oxides. In literature, these particles with squared shape have been identified as $Y_2Ti_2O_7$ [30,31].

Tensile tests performed at different temperatures up to 700°C testify that the ODS steel exhibits better mechanical properties, namely yield stress (YS) and ultimate tensile strength (UTS), than the same steel matrix (Figure 5). YS and UTS of ODS are much higher (about 40%) than those of the unreinforced steel in the range 25-400°C, at higher temperature the difference progressively decreases until 700°C where the values are quite similar. The error for each measurement is $\sim \pm 1\%$.

In order to understand this behaviour, micro-hardness and metallographic observations have been carried out on the ends (not deformed) of probes broken above 400°C and no substantial mechanical and microstructural differences were observed before and after the tensile tests. Indeed, in agreement with data reported in Table 2, the ODS hardness is not substantially affected by heat treatments in the temperature range considered here. Also fracture surfaces of probes broken at different temperatures do not display significant differences. For example, Figure 6 compares those of two probes broken in tensile tests at 400°C (Figure 6a) and 600°C (Figure 6b): the morphology with dimples typical of ductile fracture is the same in both the cases.

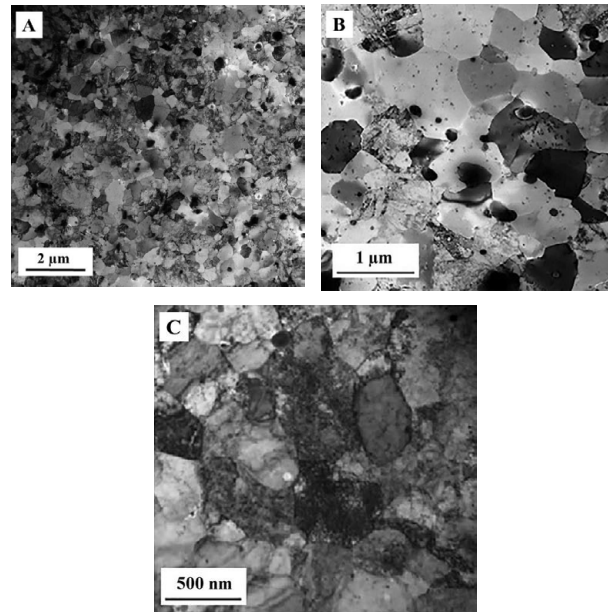


Figure 3: TEM micrographs show the microstructure of ODS steel: (a) equiaxed ferritic grains; areas with low density (b) and high density (c) of dislocations within the grains.

Particle	O	Al	Si	Ti	Cr	Fe	Y	Total Mass (%)
1	11,27	0,89	6,86	0,43	8,03	39	33,51	100
2	10,36	1,17	6,72	24,77	29,76	5,17	22,04	100
3	1,95	0,04	2,39	1,85	9,4	74,65	9,72	100
4	6,5	1,53	2,99	0,47	13,21	71,03	4,26	100
5	3,2	0,46	1,11	0,46	12,56	74,05	8,16	100

Table 3: EDX analysis of the particles 1-5 in Figure 4a.

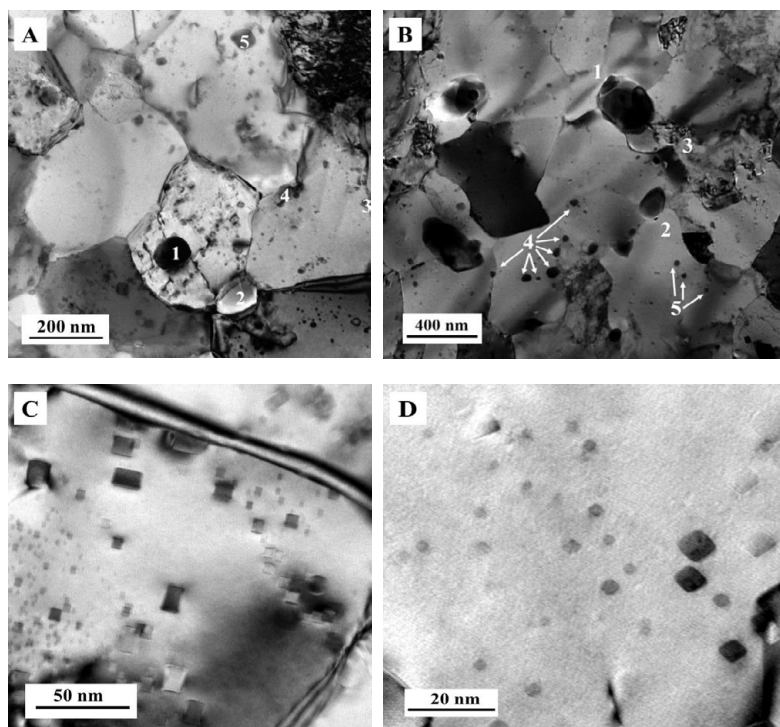


Figure 4: TEM micrographs show that two types of oxides are present in ODS steel after HE: 1-complex oxides with different amounts of alloying elements (a and b), 2-nanometric precipitates with squared shape (c and d).

Since there is no evidence of permanent changes in the structure of the material, the decrease of mechanical properties above 400°C is believed to be connected to temperature dependent mechanisms, in particular dislocation depinning from nano-particles.

Heat treated samples

In order to study the mechanical and microstructural stability of the ODS steel at high temperature, some samples have been heat treated at three different temperatures 1050, 1100 and 1150°C for 30 minutes. The hardness of heat treated samples shows a relevant decrease with respect the as-prepared material. Some data scattering is also observed in the three heat treated sets of samples (Table 4).

XRD patterns of as-prepared and heat treated material at different temperatures display a change of the relative intensities of the strongest Fe reflections, namely {110}, {200} and {211}, testifying a partial re-orientation of crystalline grains (Table 5).

XRD results are confirmed by TEM investigations. As displayed in Figure 7a, the inhomogeneity of the ferritic structure of a sample heat treated at 1150°C is evident: some of the grains show a size comparable to that of the as-prepared material (~500 nm) while other grains are much larger (~4 μm). The phenomenon can be ascribed to an uneven distribution of the nano-oxides, indeed in the areas with smaller ferritic grains the volume fraction of nano-oxides is higher compared to that of the larger grains (Figure 7b). Hence, the hardness decrease of the heat

treated samples is affected by both the grain coarsening in some regions and lower dislocation density (defect recovery).

Discussion

In order to understand how microstructure and mechanical behavior depend on different preparation routes, a comparative study of the strengthening mechanisms involved at different temperatures in the ODS steels manufactured by LEMA and HEMA has been done. In Figure 8 YS values from room temperature up to 700°C of the LEMA-ODS steel and some ODS steels, with the same nominal composition, taken from literature and prepared by HEMA are reported. The chemical composition and the manufacturing parameters are reported in Table 6.

HEMA procedure involves a final annealing treatment at high temperature (~1100°C) in order to precipitate the complex Y-Ti-O oxides. An undesired consequence of the HEMA procedure is that the high temperature annealing causes the equiaxed nanometric grains obtained by mechanical alloying to evolve towards a bimodal grain size distribution. The incomplete recrystallization and non-uniform grain growth are assumed to be the main reasons for this bimodality in grain size. In the case of LEMA, the Y-Ti-O precipitates are present in the ODS steel without the further annealing treatment and an equiaxed grain structure is exhibited.

The HEMA-ODS steels exhibit a bimodal grain size distribution

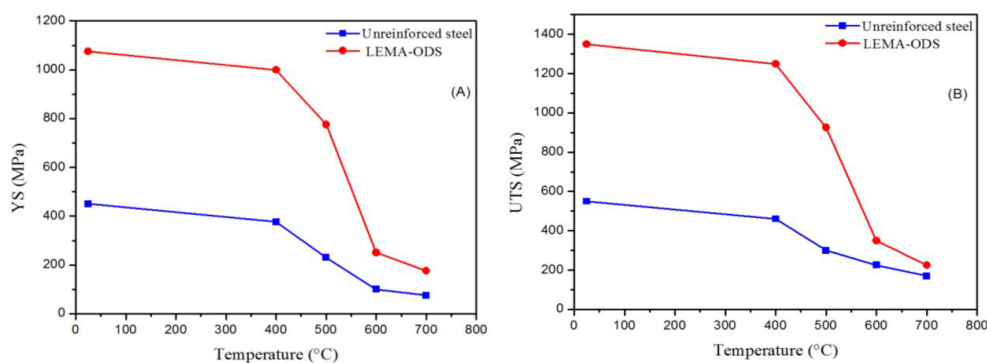


Figure 5: YS (a) and UTS (b) at increasing temperature of ODS steel are compared with those of unreinforced steel.

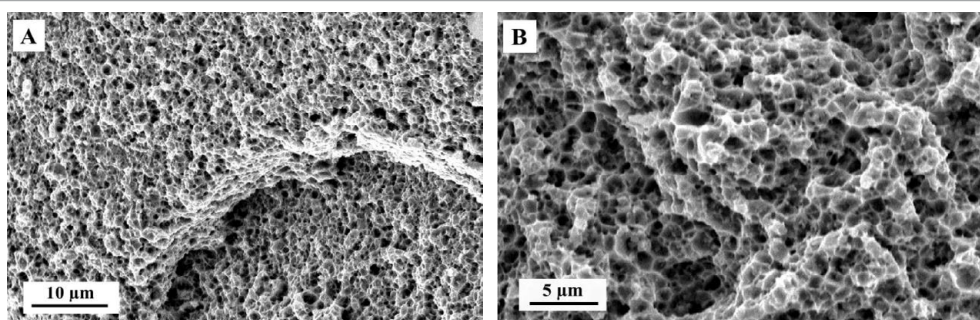


Figure 6: Fracture surfaces of probes broken in tensile tests carried out at 400°C (a) and 600°C (b).

Sample	Temperature (°C)	Time (minutes)	Hardness HV
As-prepared	No	No	447 ± 5
HE+1050°C/30 minutes	1050	30	315 ± 6
HE+1100°C/30 minutes	1100	30	327 ± 10
HE+1150°C/30 minutes	1150	30	305 ± 4

Table 4: Hardness of ODS steel in as-prepared condition and after heat treatments at three different temperatures (1050, 1100 and 1150°C) for 30 minutes.

	As-prepared	T1 (HE+1050°C/30 minutes)	T2 (HE+1100°C/30 minutes)	T3 (HE+1150°C/30 minutes)
I_{110}	100	100	100	100
I_{200}	37	41	36	49
I_{211}	43	61	50	59

Table 5: Relative intensities (normalized to 100) of the strongest Fe reflections in the XRD spectra of the as-prepared sample and heat treated ODS steel at 1050°C (T1), 1100°C (T2) and 1150°C (T3) for 30 minutes.

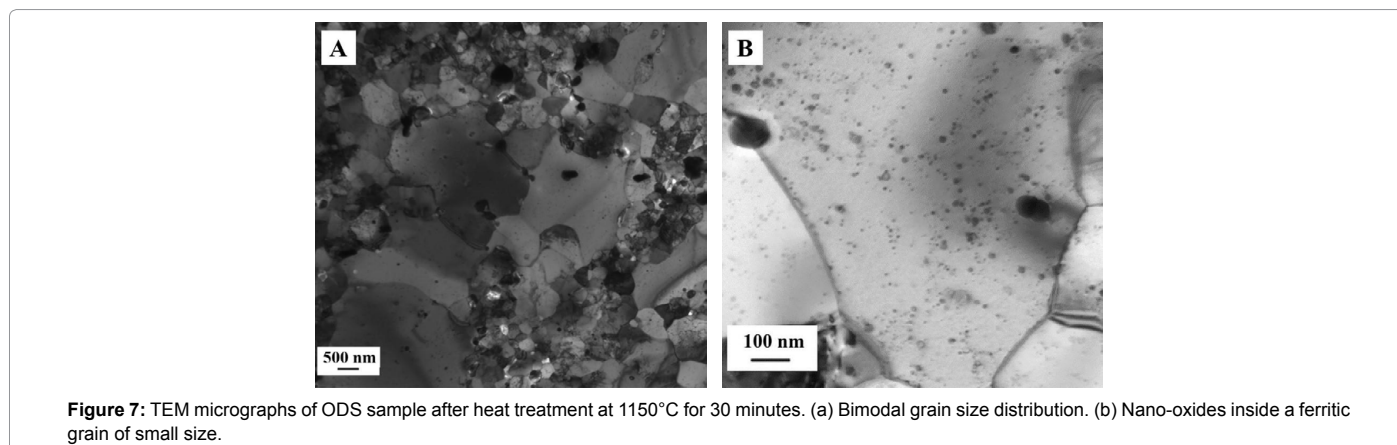


Figure 7: TEM micrographs of ODS sample after heat treatment at 1150°C for 30 minutes. (a) Bimodal grain size distribution. (b) Nano-oxides inside a ferritic grain of small size.

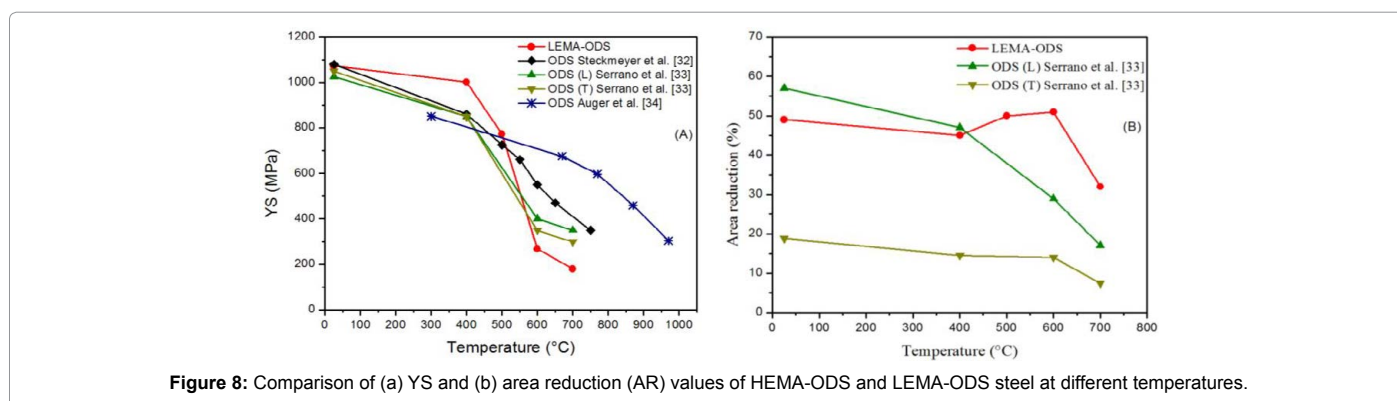


Figure 8: Comparison of (a) YS and (b) area reduction (AR) values of HEMA-ODS and LEMA-ODS steel at different temperatures.

	Composition (wt%)	Consolidation	Annealing treatment
Steckmeyer et al. [32]	Fe-14Cr-1W-0.3Ti-0.3Y ₂ O ₃	HE (1100°C)	1050°C/1 hours
Serrano et al. [33]	Fe-14Cr-1W-0.4Ti-0.3Y ₂ O ₃	HE (1100°C)	1050°C/1.5 hours
Auger et al. [34]	Fe-14Cr-2W-0.3Ti-0.3Y ₂ O ₃	HIP (1100°C)	850°C/2 hours

Table 6: Chemical composition (main alloying elements) and manufacturing parameters of HEMA-ODS steels.

and elongated grain along the extrusion direction with consequent anisotropic mechanical properties. From room temperature up to 500°C the LEMA-ODS steel exhibits higher yield strength values than the HEMA-ODS ones whereas they become lower from 500°C upwards (Figure 8a).

In Figure 8b the area reduction (AR) reported by Serrano, et al [33] along L and T directions is compared with that of LEMA-ODS at different temperatures. The HEMA-ODS steels show a higher ductility along L direction compared to T direction and higher AR (%) values along L direction up to 400°C and always lower along T direction compared to the LEMA-ODS steel prepared by authors.

HEMA-ODS steels have a bimodal grain size distribution and their YS values are equivalent or a little lower than those of LEMA-ODS from room temperature up to ~500°C when the Hall-Petch mechanism is predominant. However, at higher temperature when the component

σ_D of the Hall-Petch contribution breakdowns and is substituted by the Coble creep, the HEMA-ODS steels prepared by the conventional route exhibit better mechanical properties.

Furthermore, at lower temperatures owing to the Orowan mechanism the dislocation are forced to bypass the impenetrable precipitates but with temperature increasing the depinning of dislocation from nano-particles becomes relevant and σ_{OR} is substituted by σ_{ARW} . LEMA-ODS steel does not present a so homogeneous distribution of nanometric oxides as HEMA-ODS thus such feature is fundamental to explain the worsening of their mechanical properties above 500°C.

In order to understand the mechanical behavior depending on temperature of LEMA-ODS and unreinforced steel, the following contributions of strengthening mechanisms have been considered:

- (i) Solid solution strength (σ_{ss});
- (ii) Bailey-Hirsch strength (σ_{BH});
- (iii) Hall-Petch strength (σ_{HP});
- (iv) Orowan strength (σ_{OR});
- (v) Coble creep (σ_{CC});
- (vi) Arzt-Rösler-Wilkinson strength (σ_{ARW});
- (i) The solid solution strength (σ_{ss}) can be expressed by [35]:

$$\sigma_{ss} = 0.00689kC^n \quad (2)$$

It mainly depends on W and Cr atomic concentration C (at %). The coefficient n is 0.75 whereas k depends on the considered elements (namely W and Cr) [36].

(ii) The Bailey-Hirsch strength (σ_{BH}) can be expressed as a function of the dislocation density ρ [37]:

$$\sigma_{BH} = M\alpha Gb\rho^{1/2} \quad (3)$$

being M the Taylor factor for bcc metals, α a constant [38], G the shear modulus, b the modulus of Burgers vector. The dislocation density has been calculated by analyzing XRD peak profiles whereas the shear modulus G vs. T was measured through MS tests (Figure 9).

(iii) The Hall-Petch strength (σ_{HP}) was determined through the relationship [39,40]:

$$\sigma_{HP}(T) = \sigma_0 + \sigma_D = \sigma_0 + [G(T)/G(300K)]^{1/2} KD^{-1/2} \quad (4)$$

It is the sum of the friction stress σ_0 [41] and σ_D that mainly depends on the grain size D evaluated by TEM micrographs. Then K was calculated as $K=1/5 (G \cdot b^{1/2})$ [42].

(iv) The Orowan contribution (σ_{OR}) was calculated as [43]:

$$\sigma_{OR} = 0.9M \frac{[\ln(\pi d / b)]^{3/2} [Gb / 4\pi(1-\nu)]}{[\ln(L / b)]^{1/2} [L - (\pi d / 4)]} \quad (5)$$

being d and L the particle size and the mean spacing between particles, respectively, determined as average value of 20 TEM micrographs and ν the Poisson's ratio.

(v) At higher temperatures the Hall-Petch mechanism breakdowns and losses its efficiency [44] and the Coble creep strength (σ_{CC}) is predominant:

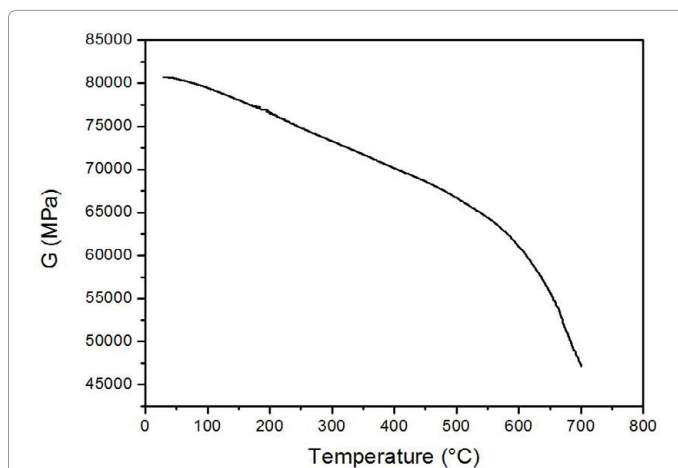


Figure 9: Shear modulus G vs. temperature determined from MS tests.

$$\sigma_{CC} = \frac{K_b TD^3 \dot{\epsilon}}{47\Omega \delta_B D_B} \exp(Q_B / RT) \quad (6)$$

where k_b is the Boltzmann constant, $\dot{\epsilon}$ the strain rate, Ω the atomic volume, $\delta_B D_B$ is the product of grain boundary width and pre-exponential factor of grain boundary diffusion, Q_B the activation energy for grain boundary diffusion and R the gas constant.

(vi) The Arzt-Rösler-Wilkinson strength (σ_{ARW}), depending on dislocation climb over hard particles, can be expressed by the following equation [45,46]:

$$\sigma_{ARW} = 0.9M \frac{R_d^{3/2}}{2\sqrt{2} + R_d^{3/2}} \frac{Gb}{L} \quad (7)$$

where R_d is the decrease of line tension of a pinned dislocation segment [47].

Therefore, the overall stress can be expressed as:

$$\sigma_y = \sigma_{ss} + \sigma_{BH} + \sigma_0 + \sigma_D + \sigma_{OR} + \sigma_{CC} + \sigma_{ARW} \quad (8)$$

Each strengthening contribution is involved at different temperature ranges.

The experimental YS data of the LEMA-ODS steel and unreinforced steel at increasing temperatures have been fitted taking into account the contributions of different strengthening mechanisms (Figure 10). The parameters are reported in Table 7.

The strengthening contributions of LEMA-ODS and unreinforced steel at increasing temperature are reported in Tables 8 and 9 respectively.

From room temperature up to 500°C, the strengthening contributions of LEMA-ODS steel are solid solution (σ_{ss}), dislocations (σ_{BH}), Hall-Petch ($\sigma_0 + \sigma_D$) and Orowan (σ_{OR}) strength. From 500°C upwards the σ_D component loses its efficiency and it is progressively substituted by the Coble creep (σ_{CC}). Furthermore, climb becomes predominant so the σ_{ARW} mechanism replaces the σ_{OR} term [32].

The main difference between LEMA-ODS steel and the unreinforced steel from room temperature up to ~500°C is the Orowan strength that leads to the better mechanical properties of LEMA-ODS

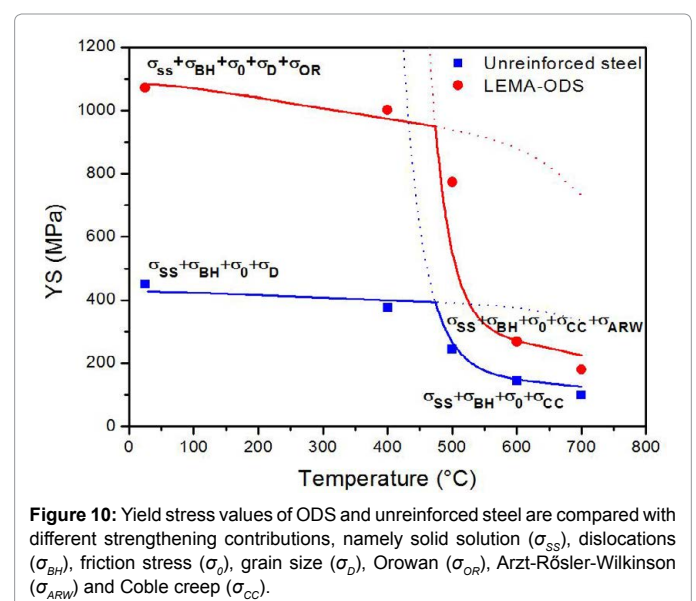


Figure 10: Yield stress values of ODS and unreinforced steel are compared with different strengthening contributions, namely solid solution (σ_{ss}), dislocations (σ_{BH}), friction stress (σ_0), grain size (σ_D), Orowan (σ_{OR}), Arzt-Rösler-Wilkinson (σ_{ARW}) and Coble creep (σ_{CC}).

Parameters	Unreinforced steel	LEMA-ODS
k_{Cr}	1400	1400
k_W	1100	1100
C_{Cr} [%at]	11	14.15
C_W [%at]	0.1	0.29
n	0.75	0.75
M	2.9	2.9
α	0.24	0.24
b [nm]	0.25	0.25
ρ [m ⁻²]	2.5×10^{13}	4×10^{12}
σ_0 [MPa]	13	13
D [μ m]	2	0.4
d [nm]	-	18
L [nm]	-	63
v	-	0.3
k_b [J/K]	1.38×10^{23}	1.38×10^{23}
$\dot{\epsilon}$ [s ⁻¹]	10^{-3}	10^{-3}
Ω [m ³]	1.18×10^{29}	1.18×10^{29}
$\delta_B D_B$ [m ³ /s]	1.1×10^{-12}	1.1×10^{-12}
Q_B [kJ/mol]	137	174
R [J/mol K]	8.31	8.31
R_d	0.77	0.77

Table 7: Parameters used to determine the contribution of each strengthening mechanism and fit experimental YS data of LEMA-ODS and unreinforced steel.

LEMA-ODS	Temperature (°C)				
Strengthening contributions to YS (MPa)	25	400	500	600	700
σ_{SS}	100	100	100	100	100
σ_{BH}	28	24	23	21	16
σ_0	13	13	13	13	13
σ_D	285	265	259	-	-
σ_{OR}	657	571	543	-	-
σ_{ARW}	-	-	133	122	94
σ_{CC}	-	-	285	16	2
$\sigma_{SS} + \sigma_{BH} + \sigma_0 + \sigma_D + \sigma_{OR}$	1083	973	938	-	-
$\sigma_{SS} + \sigma_{BH} + \sigma_0 + \sigma_{CC} + \sigma_{ARW}$	-	-	554	272	225

Table 8: Strengthening contributions to YS at 25, 400, 500, 600 and 700°C for LEMA-ODS steel.

Unreinforced steel	Temperature (°C)				
Strengthening contributions to YS (MPa)	25	400	500	600	700
σ_{SS}	75	75	75	75	75
σ_{BH}	70	61	58	53	41
σ_0	13	13	13	13	13
σ_D	268	250	244	-	-
σ_K	-	-	-	-	-
σ_{ARW}	-	-	-	-	-
σ_{CC}	-	-	128	13	2
$\sigma_{SS} + \sigma_{BH} + \sigma_0 + \sigma_D$	426	399	390	-	-
$\sigma_{SS} + \sigma_{BH} + \sigma_0 + \sigma_{CC}$	-	-	274	141	131

Table 9: Strengthening contributions to YS at 25, 400, 500, 600 and 700 °C for unreinforced steel.

whereas at higher temperatures the Arzt-Rösler-Wilkinson strength represents the main difference.

Conclusions

A ferritic nano-ODS steel with Y_2O_3 particles (0.3 wt%) has been produced by LEMA and successive HE. The microstructural features and mechanical behavior have been investigated and compared to those of the same unreinforced steel and HEMA-ODS reported in literature. The conclusions can be summarized as follows.

- (i) LEMA-ODS steel has equiaxed grains of about 400 nm

and dislocation density of $4 \times 10^{12} \text{ m}^{-2}$. Two types of second phase particles were observed: (i) round or irregular-shaped complex oxides with different contents of alloying elements, (ii) very fine oxides (few nanometers) with squared shape. Nano-oxides are stable up to 800°C and guarantee the stability of microstructure and mechanical properties.

(ii) The main difference between LEMA-ODS and the unreinforced steel from room temperature up to ~500°C is the Orowan strength leading to superior mechanical properties; at higher temperatures the Arzt-Rösler-Wilkinson strength substitutes the

Orowan one but is not as much efficient thus the mechanical properties become similar.

(iii) With respect the conventional preparation route LEMA avoids the bimodal grain size distribution. The microstructure with fine equiaxed grains involves higher and isotropic properties up to 500°C, however, the precipitate distribution in the matrix is not so homogeneous as that obtained from HEMA thus at higher temperature, where the Petch-Hall contribution breakdowns and the role played by precipitate in strengthening is dominant, YS and UTS remarkably decrease and are a little lower of those of HEMA-ODS steels.

(iv) LEMA-ODS steel heat treated above 1000°C exhibits defect recovery and partial grain growth that has been ascribed to the not homogeneous original distribution of Y_2O_3 particles.

(v) On these grounds LEMA seems a promising method, however it needs improvement to get a more homogeneous distribution of nano-oxides and consequently further enhance mechanical properties above 500°C.

References

- Duan Z, Yang H, Satoh Y, Murakami K, Kano S, et al. (2017) Current status of materials development of nuclear fuel cladding tubes for light water reactors. *Nucl Eng Des* 316: 131-150.
- Yvon P, Le Flem M, Cabet C, Seran JL (2015) Structural materials for next generation nuclear systems: Challenges and the path forward. *Nucl Eng Des* 294: 161-169.
- Tanigawa H, Gaganidze E, Hirose T, Ando M, Zinkle S, et al. (2017) Development of benchmark reduced activation ferritic / martensitic steels for fusion energy applications. *Nucl Fusion* 57: 1-13.
- Zinkle SJ, Boutard JL, Hoelzer DT, Kimura A, Odette GR, et al. (2017) Development of next generation tempered and ODS reduced activation ferritic/ martensitic steels for fusion energy applications. *Nucl Fusion* 57: 1-17.
- Gondi P, Montanari R (1992) On the Cr distribution in MANET steel. *Physica Status Solidi* 131: 465-480.
- Tan L, Katoh Y, Tavassoli AA, Henry J, Rieth M, et al. (2016) Recent status and improvement of reduced-activation ferritic-martensitic steels for high-temperature service. *J Nucl Mater* 479: 515-523.
- Gondi P, Donato A, Montanari R, Sili A (1996) A miniaturized test method for the mechanical characterization of structural materials for fusion reactors. *J Nucl Mater* 233-237: 1557-1560.
- Baluc N, Abe K, Boutard JL, Chernov VM, Diegele E, et al. (2007) Status of R&D activities on materials for fusion power reactors. *Nucl Fusion* 47: S696.
- Baluc N, Gelles DS, Jitsukawa S, Kimura A, Klueh R, et al. (2007) Status of reduced activation ferritic/martensitic steel development. *J Nucl Mater* 367: 33-41.
- Ukai S, Fujiwara M (2002) Perspective of ODS alloys application in nuclear environments. *J Nucl Mater* 307: 749-757.
- Ukai S, Okada H, Inoue M, Nomura S, Shikakura S, et al. (1993) Alloying design of oxide dispersion for long life FBRs core materials strengthened ferritic steel. *J Nucl Mater* 204: 5-73.
- Kimura A, Han W, Je H, Yabuuchi K, Kasada R (2016) Oxide dispersion strengthened steels for advanced blanket systems. *Plasma Fusion Res* 11: 1-8.
- Dadé M, Malaplate J, Garnier J, De Geuser F, Barcelo F, et al. (2017) Influence of microstructural parameters on the mechanical properties of oxide dispersion strengthened Fe-14Cr steels. *Acta Mater* 127: 165-177.
- Aydogan E, El-Atwani O, Takajo S, Vogel SC, Maloy SA (2018) High temperature microstructural stability and recrystallization mechanisms in 14YWT alloys. *Acta Mater* 148: 467-481.
- He P, Klimenkov M, Lindau R, Möslang A (2012) Characterization of precipitates in nano structured 14% Cr ODS alloys for fusion application. *J Nucl Mater* 428: 131-138.
- Klueh RL, Shingledecker JP, Swindeman RW, Hoelzer DT (2005) Oxide dispersion-strengthened steels: A comparison of some commercial and experimental alloys. *J Nucl Mater* 341: 103-114.
- Goshchitskii BN, Sagaradze VV, Shalaev VI, Arbuzov VL, Tian Y, et al. (2002) Structure, radiation resistance and thermal creep of ODS ferritic steels. *J Nucl Mater* 307: 78-3787.
- Hosemann P, Thau HT, Johnson AL, Maloy SA, Li N, et al. (2008) Corrosion of ODS steels in lead-bismuth eutectic. *J Nucl Mater* 373: 246-253.
- Chen J, Jung P, Rebac T, Duval F, Sauvag T, et al. (2014) Helium effects on creep properties of Fe-14CrWTi ODS steel at 650°C. *J Nucl Mater* 453: 253-258.
- Ding ZN, Zhang CH, Yang YT, Song Y, Kimura A, et al. (2017) Hardening of ODS ferritic steels under irradiation with high-energy heavy ions. *J Nucl Mater* 493: 53-61.
- De Carlan Y, Bechade JL, Dubuisson P, Seran JL, Billot P, et al. (2009) CEA developments of new ferritic ODS alloys for nuclear applications. *J Nucl Mater* 386: 430-432.
- Okuda T, Fujiwara M (1995) Dispersion behaviour of oxide particles in mechanically alloyed ODS steel. *J Mater Sci Lett* 14: 1600-1603.
- Eiselt CC, Klimenkov M, Lindau R, Möslang A, Sandim HRZ, et al. (2009) High-resolution transmission electron microscopy and electron backscatter diffraction in nanoscaled ferritic and ferritic-martensitic oxide dispersion strengthened-steels. *J Nucl Mater* 385: 231-235.
- Kasada R, Lee SG, Isselin J, Lee JH, Omura T, et al. (2011) Anisotropy in tensile and ductile-brittle transition behavior of ODS ferritic steels. *J Nucl Mater* 417: 180-184.
- De Sanctis M, Fava A, Lovicu G, Montanari R, Richetta M, et al. (2017) Mechanical Characterization of a Nano-ODS Steel Prepared by Low-Energy Mechanical Alloying. *Metals* 7: 1-12.
- Magini M, Iasonna A (1995) Energy transfer in mechanical alloying (overview). *Mater Trans* 36:123-133.
- Klug H, Alexander L (1974) *X-ray Diffraction Procedures for Polycrystalline and Amorphous Materials* (2nd ed) John Wiley & Sons, New York, NY, USA.
- Williamson GK, Smallman RE (1956) III. Dislocation densities in some annealed and cold-worked metals from measurements on the X-ray Debye-Scherrer spectrum. *Philos Mag* 1: 34-46.
- Amadori S, Campari EG, Fiorini AL, Montanari R, Pasquini L, et al. (2006) Automated resonant vibrating-reed analyzer apparatus for a non-destructive characterization of materials for industrial applications. *Mater Sci Eng A* 442: 543-546.
- Dawson K, Tatlock GJ (2014) Characterisation of nanosized oxides in ODM401 oxide dispersion strengthened steel. *J Nucl Mater* 444: 252-260.
- Wu Y, Ciston J, Kraemer S, Bailey N, Odette GR, et al. (2016) The crystal structure, orientation relationships and interfaces of the nanoscale oxides in nanostructured ferritic alloys. *Acta Mater* 111: 108-115.
- Steckmeyer A, Praud M, Fournier B, Malaplate J, Garnier J, et al. (2010) Tensile properties and deformation mechanisms of a 14Cr ODS ferritic steel. *J Nucl Mater* 405: 95-100.
- Serrano M, Hernández-Mayoral M, García-Junceda A (2012) Microstructural anisotropy effect on the mechanical properties of a 14Cr ODS steel. *J Nucl Mater* 428: 103-109.
- Auger MA, De Castro V, Leguey T, Monge MA, Muñoz A, et al. (2013) Microstructure and tensile properties of oxide dispersion strengthened Fe-14Cr-0.3Y2O3 and Fe-14Cr-2W-0.3Ti-0.3Y 2O3. *J Nucl Mater* 442: S142-S147.
- Li Q (2003) Modeling the microstructure-mechanical property relationship for a 12Cr-2W-V-Mo-Ni power plant steel. *Mater Sci Eng A* 361: 385-391.
- Shen J, Li Y, Li F, Yang H, Zhao Z, et al. (2016) Microstructural characterization and strengthening mechanisms of a 12Cr-ODS steel. *Mater Sci Eng A* 673: 624-632.
- Bailey JE, Hirsch PB (1960) The dislocation distribution, flow stress, and stored energy in cold-worked polycrystalline silver. *Philos Mag* 5: 485-497.
- Kocks UF, Mecking H (2003) Physics and phenomenology of strain hardening: The FCC case. *Prog Mater Sci* 48: 171-273.
- Hall EO (1951) The Deformation and Ageing of Mild Steel 3. Discussion of Results. *Proc Phys Soc London Sect B* 64: 747-753.

-
40. Petch NJ (1953) The cleavage strength of polycrystals. *J Iron Steel Inst*, pp: 25-28.
 41. Takaki S, Akama D, Nakada N, Tsuchiyama T (2014) Effect of Grain Boundary Segregation of Interstitial Elements on Hall Petch Coefficient in Steels. *Mater Trans* 55: 28-34.
 42. Praud M, Momprou F, Malaplate J, Caillard D, Garnier J, et al. (2012) Study of the deformation mechanisms in a Fe-14% Cr ODS alloy. *J Nucl Mater* 428: 90-97.
 43. Kocks UF (1977) The theory of an obstacle-controlled yield strength-Report after an international workshop. *Mater Sci Eng* 27: 291-298.
 44. Schneibel J, Heilmaier M (2014) Hall-Petch Breakdown at Elevated Temperatures. *Mater Trans* 55: 44-51.
 45. Arzt E, Wilkinson DS (1986) Threshold stresses for dislocation climb over hard particles: The effect of an attractive interaction. *Acta Metall* 34: 1893-1898.
 46. Arzt E, Rösler J (1988) The kinetics of dislocation climb over hard particles-II. Effects of an attractive particle-dislocation interaction. *Acta Metall* 36: 1053-1060.
 47. Reppich B (1998) On the attractive particle-dislocation interaction in dispersion-strengthened material. *Acta Mater* 46: 61-67.